BULLETIN OF THE POLISH ACADEMY OF SCIENCES
TECHNICAL SCIENCES, Vol. 69(4), 2021, Article number: e137727
DOI: 10.24425/bpasts.2021.137727

Predictive torque control of induction motor drive with reduction of torque and flux ripple

Babak KIANI, Babak MOZAFARI*, Soodabeh SOLEYMANI, and Hosein MOHAMMADNEZHAD SHOURKAEI

Department of Electrical Engineering, Science and research Branch, Islamic Azad University, Tehran, IRAN

Abstract. The continuing efforts to reduce the torque and flux ripples using Finite Set Model Predictive Direct Torque Control methods (FS-MPDTC) have been currently drawing great attention from the academic communities and industrial applications in the field of electrical drives. The major problem of high torque and flux ripples refers to the consideration of just one active voltage vector at the whole control period. Implementation of two or more voltage vectors at each sampling time has recently been adopted as one of the practical techniques to reduce both the torque and flux ripples. Apart from the calculating challenge of the effort control, the parameter dependency and complexity of the duty ratio relationships lead to reduced system robustness. Those are two notable drawbacks of these methods. In this paper, a finite set of the voltage vectors with a finite set of duty cycles are employed to implement the FS-MPDTC of the induction motor. Based on the so-called Discrete Duty Cycle-based FS-MPDTC (DDC-FS-MPDTC), a base duty ratio is first determined based on the equivalent reference voltage. This duty ratio is certainly calculated using the command values of the control system, while the motor parameters are not used in this algorithm. Then, two sets of duty ratios with limit members are constructed for two adjacent active voltage vectors to apply at each control period. Finally, the prediction and the cost function evaluation are performed for all the preselected voltage vectors and duty ratios. However, the prediction and the optimization operations are performed for only 12 states of the inverter. Meanwhile, time-consuming calculations related to SVM has been eliminated. So, the robustness and complexity of the control system have been respectively decreased and increased, and both the flux and torque ripples are reduced in all speed ranges. The simulation results have verified the damping performance of the proposed method to reduce the ripples of both the torque and flux and accordingly, the experimental results have strongly validated the aforementioned statement.

Key words: FS-MPTC; induction motor; duty ratio; voltage vector; torque and flux ripples.

1. INTRODUCTION

The induction motor control using dc/ac converters has become an interesting area as it pertains to the Field Oriented Control (FOC) and Direct Torque Control (DTC) [1]. Hence, different direct torque and flux control strategies are proposed for induction motors supplied by a three-level inverter [2, 3]. A DTC strategy is proposed for a three-phase induction motor fed by a three-phase direct matrix converter, while the motor's behavior can be estimated at the next sampling interval using the predictive control strategy and different matrix converter modes [4].

FOC, ST-DTC or in brief DTC controls the electrical torque and stator flux using two components of the possible voltage vectors of inverter in a stator reference frame. In addition, due to the lack of PWM block and inner current controller accompanied by the rotary coordinate conversion module, the fast dynamic response and robustness against the parameter changes make this technique an excellent alternative for FOC [5–6]. However, DTC has two notable drawbacks, i.e., high torque and flux ripples and high switching frequency. Both the DTC (due to its merits) and FOC are simultaneously considered to cope with these problems [7–10]. In this approach, two components of the reference voltage vector control the torque and flux generated by a continuous controller and bring about the constant switching frequency. Although the torque and flux ripples reduction is achieved in this method due to the use of three possible voltage vectors (two adjacent active vectors and a zero vector) of the inverter at each control cycle, the main problem of SVM based techniques is to determine the electrical torque and stator flux controllers.

Many different controllers such as proportional-integrator controllers [2, 7–9], fuzzy logic controllers [10], sliding mode controllers [11], deadbeat controllers [12] have been extensively employed to calculate the components of reference voltage vector. In addition to the use of rotary coordinate transformation, which degrades the quick dynamic response of this method as compared to the conventional DTC, the control effort is calculated through complicated and parameter dependence relations. Hence, the robustness against the parameter changes and complexity of the control system will be decreased and increased, respectively.

In recent years, FS-MPDTC has been introduced to control the torque and flux and speed by predicting the future behavior of electric drive based on its model. Like the other discrete controllers, e.g., ST-DTC, FS-MPDTC has been featured by considering the discrete nature of the actuator and employing the limited number of voltage vectors in the control algorithm. Apart from the aforementioned advantages, FS-MPDTC has much more merits, such as easy incorporation of constraints and nonlinearities in cost function and easy implementation [13].

*e-mail: mozafari@srbiau.ac.ir

Manuscript submitted 2020-12-02, revised 2021-05-01, initially accepted for publication 2021-05-20, published in August 2021

FS-MPDTC method firstly predicts all the motor variables such as the stator flux, stator current, and consequently the electrical torque for all admissible voltage vectors. Then, this method selects the switching state corresponding to the voltage vector with the lowest cost function.

Finite control-set approaches are dependent on the number of vectors applying at each control cycle, and they are categorized into three groups. These groups apply one, two or three voltage vectors in each control cycle.

Refs [14–23] are examples of one vector-based FCS-MPDTC. In [15], a formalized approach is introduced to assign the weighting factors of the objective function. The parameter dependency and high complexity are the major problems in this algorithm. Besides the aforementioned problems, one vector-based FCS-MPDTC method suffers from high torque and flux ripples and high THD.

In [18], torque and flux deadbeat controllers are employed to calculate the best effort control. Then, three adjacent feasible voltage vectors of the calculated virtual voltage vector are merely evaluated in the cost function to reduce the computational burden of the processor. However, this strategy requires many calculations to find the angle of the voltage vector satisfying the deadbeat solution. Also, this algorithm has worked correctly in the control systems with a long-time horizon.

To reduce the torque and flux ripples, the second group of FS-DTC has been recently presented. In this group, two voltage vectors, i.e., two active voltage vectors or an active voltage vector, along with a zero-voltage vector, are applied during each control period. The use of an active voltage vector along with a zero-voltage vector is known as the duty cycle control method. Some of these algorithms rely on two vector-based FS-DTC methods, which have considered the mean torque equalization [24, 25], torque deadbeat solution [26], and minimum torque ripple [27–29], Lyaupnov based duty cycle [30]. Most of the aforementioned methods focus on torque ripple reduction. However, the problem of high flux ripple, which increases the THD current, has been neglected in these works. Calculating the duty ratio algorithm and selecting the appropriate active voltage vector are the two outstanding problems of these methods. However, these methods have no appropriate steady-state performance because of the zero-voltage vector in duty ratio calculation.

In [31] and [32], some approaches are introduced to cope with this problem. In these techniques, MPDTC is firstly employed to select the optimal active voltage vector. The optimal duration of the selected vector has been accordingly computed using a torque error minimization technique. In these methods, the best active voltage vector is selected based on the plausible assumption that will apply the whole control cycle, whereas the time of this application varies with the change of the duty cycle. Hence, the selected voltage vector may no longer be an optimum choice. However, the separate selection of active voltage vector and its relevant duty ratio leads to weak operational performance, especially at low speed.

A simultaneous determination of optimal voltage considering its duration time has been presented in [33] to tackle the cascaded selection of the best voltage vector and its corresponding duty ratio. The duty ratio of any feasible voltage vectors is calculated based on the torque deadbeat solution at the beginning of the MPTC loop, and prediction is subsequently carried out for the selected voltage vector and calculated duty ratio. Note that the duty cycle control produces the virtual voltage vectors with just different lengths in the direction of the basic voltage vectors of the inverter. These virtual voltage vectors with different amplitudes can be employed to reduce the only one of torque or flux ripples.

The idea of combining two feasible voltage vectors of a 2-level voltage source inverter (2L-VSI) has been introduced to overcome this problem [34]. Hence, this comprehensive two-vector based algorithm produces different vectors based on basic voltage vectors with different duration times. Since the diversity of voltage vectors is significantly increased, it is expected that the ripples of both electrical torque and stator flux to be reduced at the same time. However, apart from that the cost function evaluation, it has to be performed 25 times in each sampling period that the duty ratio relationship is very complicated considering all motor parameters. Consequently, these problems decrease and increase the robustness and complexity of the control system, respectively.

Three-vector based FS-DTC methods are the appropriate choices to reduce both the torque and flux ripples significantly, and it is expected that they can compete with the SVM based methods.

In [35], two constant values duty ratios are firstly considered for two active voltage vectors. Then, these vectors, along with a zero-voltage vector, are applied to the motor. Since the duty ratios are just two constant values, the minimum ripple cannot be achieved in all speed ranges.

In this paper, a three-vector (two active vectors and one zero vector) based DDC-FS-MPDTC method is introduced to cope with the problems of the prior DTC-based algorithms. The first active voltage vector is selected from the members of the preselected set, where the members of the aforementioned set are selected among the feasible active voltage vectors of 2L-VSI based on a switching pattern that compare the estimated and reference values of the electrical torque. Also, the second vector is the next adjacent vector of the first selected vector. In the next step, the reference of BEMF is calculated using the command values of the rotor speed and stator flux. The equivalent reference voltage and the maximum voltage produced by the inverter are the determinative factors of a base duty ratio. Then, a set of new duty ratios is determined as the resultant duty ratios according to the base duty ratio. The duty ratios of the preselected active voltage vectors and their next ones are computed by the employment of the equivalent duty ratios. Finally, DDC-FS-MPDTC is employed for all preselected voltage vectors and the proposed method's duty ratios.

Since the selected duty ratios are entirely independent of the motor parameters, this method is most robust against the parameter variations. Also, the proposed method does not consider any especial principle for torque or flux ripples reduction alone, and a parameter determines the relative importance of torque and flux control concerning each other by weighting factor. Hence, both the electrical torque and stator flux ripples are

simultaneously reduced in the proposed method. Other sections can be summarized as follows:

The induction motor and inverter have been modelled in section 2. The proposed discrete duty cycle based torque and flux control strategy has been described in section 3. Section 4 has analytically compared the proposed method and one of the most comprehensive duty cycle-based methods. The simulation and experimental results are respectively provided in Sections 5 and 6.

2. MODELS OF INDUCTION MOTOR AND INVERTER

The mathematical model of the induction motor in the stationary reference frame is expressed as follows.

$$\vec{v}_s^i = R_s\vec{I}_s + \frac{d\vec{\psi}_s}{dt}, \tag{1}$$

$$\vec{v}_s^i = R_r\vec{I}_r + \frac{d\vec{\psi}_r}{dt} - j\omega_r\vec{\psi}_r, \tag{2}$$

$$\vec{\psi}_s = L_s\vec{I}_s + L_m\vec{I}_r, \tag{3}$$

$$\vec{\psi}_r = L_m\vec{I}_s + L_r\vec{I}_r, \tag{4}$$

$$\frac{d\omega_r}{dt} = \frac{P}{2J}(T_e - T_m), \tag{5}$$

$$T_e = \frac{3P}{4}\Im m\left(\vec{I}_s\,\vec{\psi}_s^*\right), \tag{6}$$

where $\vec{\psi}_s$ and $\vec{\psi}_r$ are the stator and rotor flux vectors, respectively. $\vec{I}_s$ and $\vec{I}_r$ are the stator and rotor current vectors, respectively. ω_r is the rotor angular frequency. T_m and T_e are respectively the mechanical and electrical torques. L_m, L_s and L_r are respectively the mutual, stator and rotor inductances, R_s and R_r are respectively the stator and rotor resistances, P is the number of poles, and J is the moment of inertia.

Also, $\vec{v}_s^i$, is the stator voltage vector, where $i = 1,\ldots,6$. The 2L-VSI produces these six active voltage vectors, and also, two zero voltage vectors along with their relevant switching states are presented in Fig. 1.

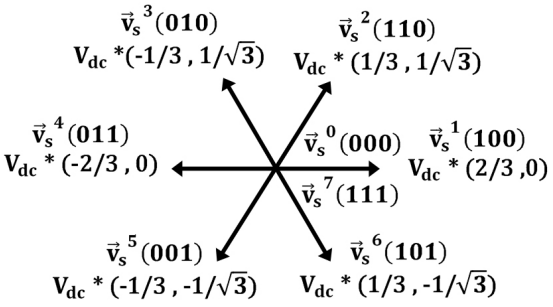

Fig. 1. Switching states and voltage vectors of inverter

$\vec{v}_s^i$ is given as follows:

$$\begin{aligned}\vec{v}_s^i &= \frac{2}{3}V_{dc}\exp\left(i\frac{\pi}{3}\right)\\ &= \frac{2}{3}\cos\left(i\frac{\pi}{3}\right)V_{dc} + j\frac{2}{3}\sin\left(i\frac{\pi}{3}\right)V_{dc}\\ &= \mathrm{dir}\,v_d^i\cdot V_{dc} + j\mathrm{dir}\,v_q^i\cdot V_{dc}, \qquad i = 1,2,\ldots,6.\end{aligned}$$

Also, $\vec{v}_s^i$ in terms of d and q components is presented as follows:

$$\vec{v}_s^i = v_d^i + jv_q^i, \tag{7}$$

$$v_d^i = \mathrm{dir}\,v_d^i V_{dc}, \tag{8}$$

$$v_q^i = \mathrm{dir}\,v_q^i V_{dc}, \tag{9}$$

where $\mathrm{dir}\,v_d^i$ and $\mathrm{dir}\,v_q^i$ determine the direction of the inverter voltage vectors, and V_{dc} is the dc-link voltage of the 2L-VSI.

3. PRINCIPLE OF THE PROPOSED METHOD

This paper presents an effective and parameter-dependent duty cycle based MPDTC to reduce both the torque and flux ripples. In this algorithm, as soon as measuring the stator current and dc-link voltage, the motor's variables are estimated by a sliding mode observer. A preselection mechanism reduces the number of voltage vectors in the next stage. Then, prediction is performed by replacing all the candidate voltage vectors and two sets of duty ratios in the motor model. These two duty ratio sets are selected based on the equivalent reference voltage. Finally, the cost function evaluation is done, and the optimal voltage vectors and their two respective duty ratios are selected. The overall control diagram of the proposed algorithm is shown in Fig. 2, which has been discussed in detail in this section.

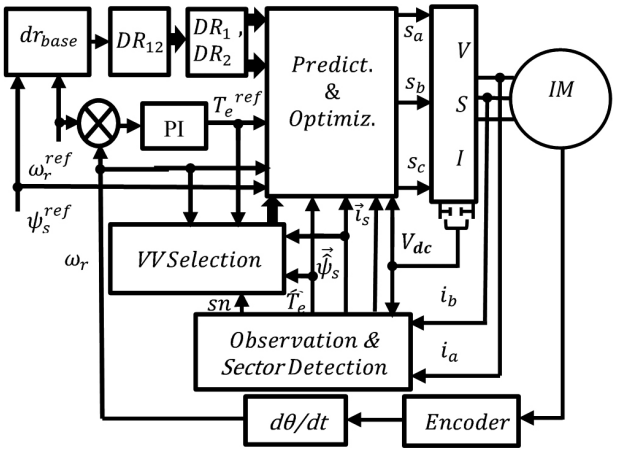

Fig. 2. Control diagram of the proposed strategy

3.1. Estimation of motor variables

In this work, due to the lack of the dc offset and drift in a full order observer compared to a simple estimator, a full order observer is employed to estimate the induction motor's variables. Also, replacing a sliding mode observer instead of a proportional observer enhances the accuracy and robustness of the proposed estimator against parameter changes in a wide speed range. Therefore, a full order sliding mode observer is a final alternative used in this paper. Stator and rotor currents are chosen as the state variables for the proposed observer. The state-space equations of induction motor in terms of new state variables are obtained by substituting (3), (4) in (1), (2) with more simplifications and are introduced as

$$\dot{\vec{X}} = A\vec{X} + B\vec{v}_s + K_o\,\mathrm{sign}\left(\vec{I}_s - \hat{\vec{I}}_s\right), \tag{10}$$

where, $\vec{X} = \left[\vec{I}_s \;\; \vec{I}_r\right]^T$, $\vec{v}_s = \vec{veq}_s^i$ is the voltage vector applied in the previous time instant, $\lambda = 1/(L_s L_r - L_m^2)$, and

$$A = \lambda \begin{bmatrix} -R_s L_r - j\omega_r L_m^2 & R_r L_m - j\omega_r L_r L_m \\ R_s L_m + j\omega_r L_s L_m & -R_r L_s + j\omega_r L_r L_s \end{bmatrix}, \tag{11}$$

$$B = \begin{bmatrix} \lambda L_r \\ -\lambda L_m \end{bmatrix}, \tag{12}$$

$$\dot{\vec{X}}_s = \left[\dot{\vec{I}}_s \;\; \dot{\vec{I}}_r\right]^T, \tag{13}$$

$$K_o = \begin{bmatrix} k_{o1} \\ k_{o2} \end{bmatrix} = \begin{bmatrix} k_{1\text{real}} + j\omega_r k_{1\text{imag}} \\ k_{2\text{real}} + j\omega_r k_{2\text{imag}} \end{bmatrix}. \tag{14}$$

Also, K_o is the observer constant gain matrix and its real and imaginary components are calculated in simulations as introduced in [36]. Finally, rotor flux, stator flux, and electrical torque are estimated as follows.

$$\vec{\psi}_s = L_s \vec{I}_s + L_m \vec{I}_r, \tag{15}$$

$$\vec{\psi}_r = L_m \vec{I}_s + L_r \vec{I}_r, \tag{16}$$

$$\hat{T}_e = \frac{3P}{4} \Im m \left(\vec{I}_s \, \vec{\psi}_s^*\right). \tag{17}$$

Components of $\vec{veq}_s^i$ are calculated as

$$veq_d^i = \text{dir}\, veq_d^i V_{dc} \tag{18}$$

$$veq_q^i = \text{dir}\, veq_q^i V_{dc}, \tag{19}$$

where $\text{dir}\, veq_d^i$, and $\text{dir}\, veq_d^i$ in all cases, one, two, and three vectors (two active and a zero vector) control are calculated as follows.

$$\text{dir}\, veq_d^i = \sum_{j=1}^{m} \left(\text{dir}\, v_d^j t_j\right)/T_s, \tag{20}$$

$$\text{dir}\, veq_q^i = \sum_{j=1}^{m} \left(\text{dir}\, v_q^j t_j\right)/T_s, \tag{21}$$

where t_j is the voltage vector duration, T_s is the sampling period, and m is the number of applied voltage vectors in each sampling period.

3.2. Selecting two sets of candidate voltage vectors using a switching table

In the FCS-MPDTC method, all feasible voltage vectors produced by the power converter must be evaluated in the cost function. This problem leads to significant growth in the computational burden of the processor. Comparing the estimated and command torque can be used to select the appropriate candidate voltage vectors among all feasible ones of the converter. The candidate voltage vectors are selected based on the stator flux position, which is expressed in terms of sector number, and shown in Fig. 3.

Also, the required calculations for determining the flux sector number are shown in this diagram with no repetitious illustration. In this paper, a bidirectional table is presented to investigate the effect of voltage vectors and the variations of torque and flux on each other, which is shown in Table 1.

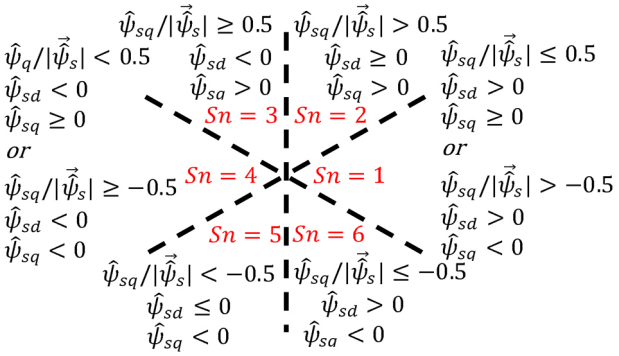

Fig. 3. Stator flux sector determination

Table 1
Analysis and design table of DTC in counter clockwise rotation (the sector number of flux vector is *sn*)

	$\vec{v}_s^{sn}$	$\vec{v}_s^{sn+1}$	$\vec{v}_s^{sn+2}$	$\vec{v}_s^{sn+3}$	$\vec{v}_s^{sn+4}$	$\vec{v}_s^{sn+5}$
$e_{\vert\vec{\psi}_s\vert}$	0	+	+	0	–	–
e_{T_e}	+	+	–	–	–	+

To investigate this switching table, the voltage vectors $\vec{v}_s^7 \ldots \vec{v}_s^{12}$, respectively equivalent with $\vec{v}_s^1 \ldots \vec{v}_s^6$ are first introduced. The concept of DTC is that the tangential component of each feasible voltage vector of the inverter, which is perpendicular to the stator flux vector, changes the electrical torque and the components that align to the flux vector changes the flux amplitude. Note that each voltage vector's effect over the torque and flux variations is discussed in the analysis case and is not investigated here. However, in the case of design, the torque error and the stator flux error are firstly defined as follows.

$$e_{T_e} = T_e^{\text{ref}} - \hat{T}_e, \tag{22}$$

$$e_{|\vec{\psi}_s|} = \psi_s^{\text{ref}} - \left|\vec{\hat{\psi}}_s\right|, \tag{23}$$

where, T_e^{ref}, ψ_s^{ref} are the torque and flux command values, respectively. Now, suppose that the motor rotates in the counter clockwise direction. An example of a design case is here presented. If both e_{T_e} and $e_{|\vec{\psi}_s|}$ are negative, then $\vec{v}_s^{sn+4}$ will be selected from the switching table. The sector number of flux vector is equal to 5 ($sn = 5$), $\vec{v}_s^{5+4} = \vec{v}_s^3$ is selected. According to Table 1, half of the voltage vectors increase the electrical torque, and another half decrease it. Therefore, there is no need for performing torque and flux prediction and cost function evaluation for all feasible voltage vectors of the inverter.

Consequently, prediction is performed for three feasible voltage vectors of the inverter that decrease or increase the electrical torque. Finally, dependent on the direction of rotation and sign of e_{T_e}, $\vec{v}_s^{sn}$, $\vec{v}_s^{sn+1}$ and $\vec{v}_s^{sn+2}$ or $\vec{v}_s^{sn+3}$, $\vec{v}_s^{sn+4}$ and $\vec{v}_s^{sn+5}$ must be selected and applied as the first voltage vector. Also, the following adjacent vector of the first selected vector is considered as the second vector.

3.3. Model-based prediction of the motor variables

The induction motor model must be discretized in digital implementation to predict the required variables such as stator flux and electrical torque in the next sampling instant. Noted that, because of the processing time of the control algorithm, there is one step delay between the applied voltage vector and the selected vector in real-time application. Therefore, two-step compensations are employed to compensate for this delay time. In this technique, $\vec{I}_s(k+1)$, $\vec{I}_r(k+1)$, $\vec{\psi}_s(k+1)$ and $\vec{\psi}_r(k+1)$ at $(k+1)$-th instant are first presented, and they are considered the initial points to calculate the torque and flux $(k+2)$-th instant. Two steps ahead, a prediction must be made. This will be achieved through the forward Euler approximation as follows.

$$\vec{X}(k+1) = \vec{X}(k) + T_s\left(A\vec{X}(k) + B\vec{v}_s(k)\right), \tag{24}$$

where, $\vec{X}(k+1) = \left[\vec{I}_s(k+1)\ \ \vec{I}_r(k+1)\right]^T$ is the predicted current matrix, and voltage vector $\vec{v}_s(k)$ is variable has been used in the observation stage.

$$\vec{\psi}_s(k+1) = L_s\vec{I}_s(k+1) + L_m\vec{I}_r(k+1), \tag{25}$$

$$\vec{\psi}_r(k+1) = L_m\vec{I}_s(k+1) + L_r\vec{I}_r(k+1). \tag{26}$$

After predicting variables at $(k+1)$-th time instant, the prediction at $(k+2)$-th time instant has to be performed. However, prediction is made for all candidate voltage vectors $\vec{v}_s^i$ at this time. This stage can be expressed as follows.

$$\vec{X}^i(k+2) = \vec{X}(k+1) + T_s\left(A\vec{X}(k+1) + B\vec{v}_s^i(k+1)\right), \tag{27}$$

where, $\vec{X}^i(k+2) = \left[\vec{I}_s^i(k+2)\ \ \vec{I}_r^i(k+2)\right]^T$. In fact, $\vec{X}$ is replaced by $\vec{X}^i$.

Similarly to the first step prediction, $\vec{\psi}_r^i(k+1)$ and $\vec{\psi}_s^i$ at $(k+1)$ can be calculated by:

$$\vec{\psi}_r^i(k+2) = L_m\vec{I}_r^i(k+2) + L_r\vec{I}_r^i(k+2), \tag{28}$$

$$\vec{\psi}_s^i(k+2) = L_s\vec{I}_s^i(k+2) + L_m\vec{I}_r^i(k+2). \tag{29}$$

Finally, the predicted electrical torque is calculated as follows:

$$T_e^i(k+2) = \frac{3P}{4}\Im m\left(\vec{I}_s^i(k+2)\vec{\psi}_s^{i\,*}(k+2)\right). \tag{30}$$

Prediction is performed for all resultant voltage vectors and will be achieved using (23)–(27).

3.4. Duty ratio calculations

Considering just one voltage vector at each sampling interval time in discrete control-based methods leads to a high level of torque and flux ripples in electrical drives. A much more enhanced category of discrete control-based methods applying two or more voltage vectors at each control period is known duty cycle control technique. Various torque and flux ripple reduction criteria can be employed to determine the duty ratios of voltage vectors. In the best case, the synthesis of two active voltage vectors and a zero-voltage vector provided enough freedom to reduce both the torque and flux ripple. The increase of the motor speed increases the partial voltage of the motor dc-link. This means that the duty ratio must be increased. So, a basic duty ratio is primarily introduced according to the equivalent voltage concept. Since the internal voltage of the motor is about multiplying the stator flux in speed. Thus, any increase in motor speed means an increase of the equivalent voltage of the motor. Hence, it should allocate a greater proportion of the input voltage, that ratio of the equivalent voltage to the input voltage, or duty cycle reaches unity (close to 1), so it is easily determined away from any complexity of the duty cycle. It will be discussed in detail as follows:

To investigate duty ratio determination, the equivalent reference voltage can be essentially expressed as follows.

$$E = \omega_s\psi_s^{\text{ref}}, \tag{31}$$

where ω_s is the angular frequency of motor variables in steady-state operation. By substituting ω_r^{ref} and ω_{slip} in (28) and introducing the BEMF, the following equation can be attained:

$$E_{\text{ref}} = \psi_s^{\text{ref}}\left(\omega_r^{\text{ref}} + \omega_{\text{slip}}\right), \tag{32}$$

where E_{ref} is the equivalent voltage and this voltage is a fraction of $v_{m\_\max}$.

Where $v_{m\_\max}$ (nominal voltage) is equivalent to nominal speed. This means that if $\omega_r^{\text{ref}} = \omega_{r\_\max}^{\text{ref}}$ then $E_{\text{ref}} = v_{m\_\max}$.

So, the base duty ratio can be presented as follows:

$$dr_{\text{base}} = E_{\text{ref}}/v_{m\_\max}, \tag{33}$$

By substituting (29) into (30), dr_{base} can be achieved by:

$$dr_{\text{base}} = \psi_s^{ref}\left(\omega_r^{\text{ref}} + \omega_{\text{slip}}\right)/v_{m\_\max}, \tag{34}$$

where V_{dc} has to meet the following inequality.

$$V_{dc} \geq \sqrt{3}v_{m\_\max}. \tag{35}$$

Consequently, by tuning $V_{dc} = \sqrt{3}v_{m\_\max}$, the base duty ratio cab be calculated as follows:

$$dr_{\text{base}} = \left(\sqrt{3}\psi_s^{\text{ref}}\left(\omega_r^{\text{ref}} + \omega_{\text{slip}}^{\max}\right)\right)/V_{dc}, \tag{36}$$

where $\omega_{\text{slip}}^{\max}$ is the slip speed in nominal speed and nominal torque.

Where $DR_{1,2}$ is defined as equivalent duty ratio vector, where its elements are determined as follows.

$$DR_{1,2}(m) = (1-(m-1)*\Delta DR_{1,2})*dr_{\text{base}}, \tag{37}$$

where $\Delta DR_{1,2} = 0.4$, m is the voltage vector counts in each iteration, and $m = 1,\ldots,M$.

Where M is the number of selected duty ratios for the first active voltage vector and in this paper, $M = 2$.

It should be noted that large and small values of $\Delta DR_{1,2}$ lead to high torque and flux ripples, especially in the nominal speed and torque.

By a similar approach, the duty ratios related to the first active voltage vector, namely the members of DR_1 are calculated as follows:

$$DR_1(n) = DR_{1,2}(m) - (n-1)*\Delta DR_1, \tag{38}$$

where $\Delta DR_1 = 0.4$, n is the voltage vector counts in each iteration, and $n = 1,\ldots,N$.

Where N is the number of selected duty ratios for the second active voltage vector and in this paper, $N = 2$.

The value of 2 for M and N is the minimum value that could be selected because only one of the two operating periods is selected. Selecting values greater than 2, although it reduces the flux and torque ripples, this reduction is not noticeable to increase M, and the algorithm merely expenses additional time for it.

The elements of the second active voltage vector, namely the members of DR_2 are calculated as follows:

$$DR_2(n) = DR_{1,2}(m) - DR_1(n). \tag{39}$$

The rest of the sampling period is allocated to the zero vector, which is written at below:

$$t_0(n) = (1 - DR_1(n) - DR_2(n)) * T_s\,. \tag{40}$$

Since low numbers of both voltage vectors and duty ratios are considered in this paper, only 12 states are evaluated in the prediction loop of the proposed algorithm. This limited number of combined states leads to a significant decrease in the computational burden of the processor. In accordance with the processor's power, the increment step of duty ratios, i.e., ΔDR_1, $\Delta DR_{1,2}$ can be decreased, and M, N can be increased. Therefore, torque and flux ripples will be considerably reduced.

3.5. Cost function Evaluation and Optimal voltage vector selection along with their respective duty ratios

In FS-MPDTC, the cost function is presented to find the optimal voltage vector. The cost function can be included in several terms. Tracking of torque and flux are the two main terms of the cost function. Over-current protection can be added to the cost function as an important constraint. Finally, the overall cost function can be expressed as follows:

$$CF_i = \left(T_e^{\text{ref}} - T_e^i(k+2)\right)^2 + \rho\left(\psi_s^{\text{ref}} - \left|\vec{\psi}_s^i(k+2)\right|\right)^2 + I_{\text{lim}}^2\,, \tag{41}$$

where ρ is the weighting factor, which determines the relative importance of torque tracking and flux tracking with respect to each other, this parameter is taken from Ref. [37]. I_{lim}^2 is included in the cost function to protect the motor against overcurrent and can be defined by:

$$I_{\text{lim}}^2 = \begin{cases} 0 & \left(I_s^i(k+2)\right)^2 \le I_{\max}^2\,, \\ \xi \gg 0 & \left(I_s^i(k+2)\right)^2 < I_{\max}^2\,, \end{cases} \tag{42}$$

where $I_{\max}^2$ is the square of maximum stator current, and $(I_s^i(k+2))^2$ can be calculated as follows:

$$\left(I_s^i(k+2)\right)^2 = \left(I_{sd}^i(k+2)\right)^2 + \left(I_{sq}^i(k+2)\right)^2. \tag{43}$$

To more conceive, the proposed control strategy in one control cycle can be summarized by the signal flow graph presented in Fig. 4.

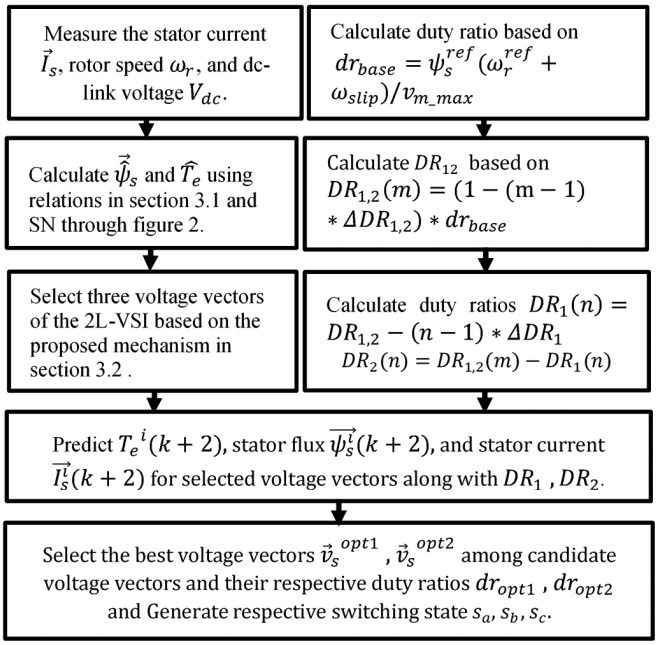

Fig. 4. Graphical representation of the proposed method

4. ANALYTICAL COMPARISON WITH GENERALIZED TWO-VECTOR-BASED ALGORITHM

One of the most specific techniques in the field of duty cycle control has been introduced in [34]. The algorithm presented in this method employs two voltage vectors at each control cycle. This method is a comprehensive form of [33]. In [34], two active voltage vectors and their respective duty ratios are determined based on the deadbeat response principle of the electrical torque. In this paper the time duration of two active voltage vectors $\vec{u}_1$ and $\vec{u}_2$ are obtained as follows

$$t_1 = \frac{\left(T_e^{\text{ref}}/0.75P\right) - \hat{T}_e - T_s\left(I_{s\lambda q}u_{2d} - I_{s\lambda d}u_{2q}\right)}{I_{s\lambda q}\left(u_{1d} - u_{2d}\right) + I_{s\lambda d}\left(u_{1q} - u_{2q}\right)}\,, \tag{44}$$

$$t_2 = T_S - t_1\,. \tag{45}$$

To determine the duty ratios, an estimation of predicted current is necessary. Hence, $\vec{I}_{s\lambda}$ must be calculated as follows.

$$\vec{I}_{s\lambda} = (1 - \lambda R_r L_s T_s + j\omega_r T_s)\vec{I}_s + \lambda\left(R_r T_s - L_r - j\omega_r L_r T_s\right)\vec{\hat{\psi}}_s\,. \tag{46}$$

The presented strategy has the following disadvantages in comparison with our proposed method.

1. In [34], around twenty-five combinations of voltage vectors must be evaluated in the prediction loop beside the complicated duty ratio calculations. Therefore, the computational burden of the processor is extensively increased. In contrast, the proposed method has been evaluated for three combinations of voltage vectors and four duty ratios in the control loop. Consequently, prediction and cost function evaluation are merely performed twelve times (around half of the time [34]).
2. In [34], the duty ratio is calculated through a complicated relationship depending on the motor parameters. This high parameter dependency deteriorates the robustness and leads to

a high level of complexity in the control strategy. Whereas, in the proposed method, the duty ratios are obtained based on reference variables. So, robustness against parameter changes is very high, and complexity is low in the proposed method.

3. The method introduced in [34] relies on torque deadbeat response. However, flux ripple reduction is achieved along with applying the torque deadbeat solution. Nevertheless, the proposed method reduces both ripples of stator flux and electrical torque concurrently without considering any principle for reducing the torque or flux ripples.

5. SIMULATION STUDY

A series of simulation studies verify the superiority of the proposed strategy. These simulations have been executed in the environment of MATLAB/Simulink. Classical DTC, MPDTC [21], MPDTC with optimal duty ratio [33], and the proposed method will be compared in detail in this section. For simplicity, the method in [33] is named Duty-MPDTC. The time duration of each control cycle in the proposed method is considered 80 μs for all simulations. In the other methods, sampling frequencies are increased to achieve the same switching frequencies. The motor and controller parameters have been shown in Table 2.

Table 2
Parameters of the system used in this paper

R_s	Stator resistance	10.8 Ω
R_r	Rotor resistance	15 Ω
L_s	Stator inductance	0.477 H
L_r	Rotor inductance	0.477 H
L_m	Mutual inductance	0.435 H
J	Moment of inertia	0.000152 kg m^2
P	Number of poles	4
P_{out}	Rated power	0.75 kW
T_{rated}	Rated torque	4 Nm
ω_{rated}	Rated speed	1390 rpm
ψ_s^{ref}	Flux amplitude reference	0.87 Wb
V_{dc}	DC-link rated voltage	540 V

In this study, the value of the weighting factor is set to 100, which is used in [40]. The stator flux reference is tuned at 0.87 Wb, which is lower than the rated value of 0.94 Wb. This reduction in reference flux is considered to prevent magnetic saturation. Finally, the value of the maximum slip is adjusted to 55 rad/s. Meanwhile, Torque ripple and flux ripple indexes are calculated as follows.

$$T_{e\_\text{rip}} = \sqrt{(1/N)\sum_{it=1}^{N}\left(T_e(it) - T_{e\_\text{av}}\right)}, \tag{47}$$

$$\psi_{s\_\text{rip}} = \sqrt{(1/N)\sum_{it=1}^{N}\left(|\vec{\psi}_s(it)| - \psi_{s\_\text{av}}\right)}, \tag{48}$$

where T_{e_rip}, and ψ_{s_rip}, are the electrical torque ripple index and stator flux ripple index. Also, T_{e_av} and ψ_{s_av} are respectively the average values of torque and stator flux. Meanwhile, N is the number of samples. The performance of stator current has been evaluated through the THD criterion, which is given by:

$$THD = \frac{I_{\text{rms}\_h}}{I_{\text{rms}\_1}} * 100, \tag{49}$$

$$I_{\text{rms}\_h} = \sqrt{\left(I_{\text{rms}}^2 - I_{\text{rms}\_1}^2\right)}, \tag{50}$$

where I_{rms}^2, and $I_{\text{rms}\_1}^2$ are the root mean square (RMS) values of the stator current and its fundamental component, respectively.

In the first simulation, the steady-state performance of DTC, MPDTC, Duty-MPDTC, and the proposed method has been performed. Figure 5 presents results of high-speed operation 1500 rpm under nominal torque. It can be seen, the proposed method exhibits much better performance in terms of torque and flux ripples reduction. Also, current THD is remarkably lower than other methods.

Figure 6 presents the simulated steady-state responses at 150 rpm with nominal torque for four understudy methods. As for that, the conventional DTC presents very high torque and flux ripples with high current harmonics. MPDTC and Duty-MPDTC relatively present high torque and flux ripple with respect to the proposed method. Duty-MPDTC, due to implement the torque dead beat response, has the lowest torque ripple.

The harmonic spectra of stator current at 150 rpm have been shown in Fig. 7. In this figure, THD has been presented up to 8000 Hz. It is seen that the current THD of the proposed method is only 0.05%, which is lower than the THD of other methods.

The proposed method exhibits the best steady-state performance in terms of torque and flux ripples and stator current harmonics, confirming the proposed method's effectiveness. Table 3 and Table 4 present the summarized results in the low and high-speed operations that confirm the effectiveness of the proposed method. Subsequently, Figs. 8 and 9 are the stator flux locus of all understudy methods at low and high-speed performance. As shown, the stator flux locus of the proposed method presents good results in terms of shape and smoothness com-

Table 3
Simulated results at 1500 rpm with 4 Nm load

Method	f_{ave} (kHz)	T_{e_rip} (%)	ψ_{s_rip} (%)	THD (%)
DTC	16.42	3.5	0.57	4.8
MPDTC	16.84	4	0.78	3.8
Duty-MPDTC $f_s = 16$ kHz	16.26	2.5	0.82	3.1
Proposed method $f_s = 12.5$ kHz	16.66	2.4	0.52	2

Table 4
Simulated results at 150 rpm with 4 Nm load

Method	f_{ave} (kHz)	T_{e_rip} (%)	ψ_{s_rip} (%)	THD (%)
DTC	16.42	6.7	0.086	5.93
MPDTC	16.84	2.2	0.05	2.72
Duty-MPDTC $f_s = 16$ kHz	16.26	0.02	0.025	0.09
Proposed method $f_s = 12.5$ kHz	16.66	0.2	0.021	0.05

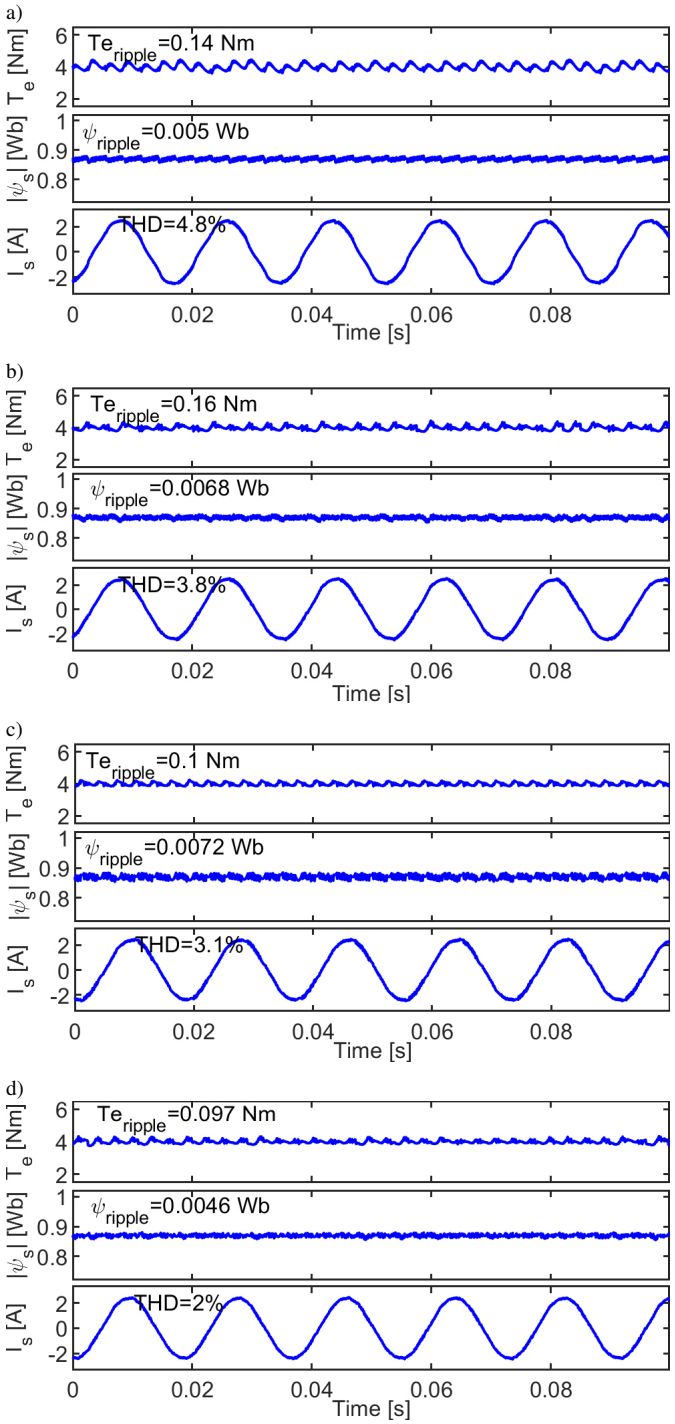

Fig. 5. Simulated steady-state response at 1500 rpm with rated torque (4 Nm): a) DTC, b) MPDTC, c) Duty-MPDTC, and d) the proposed method

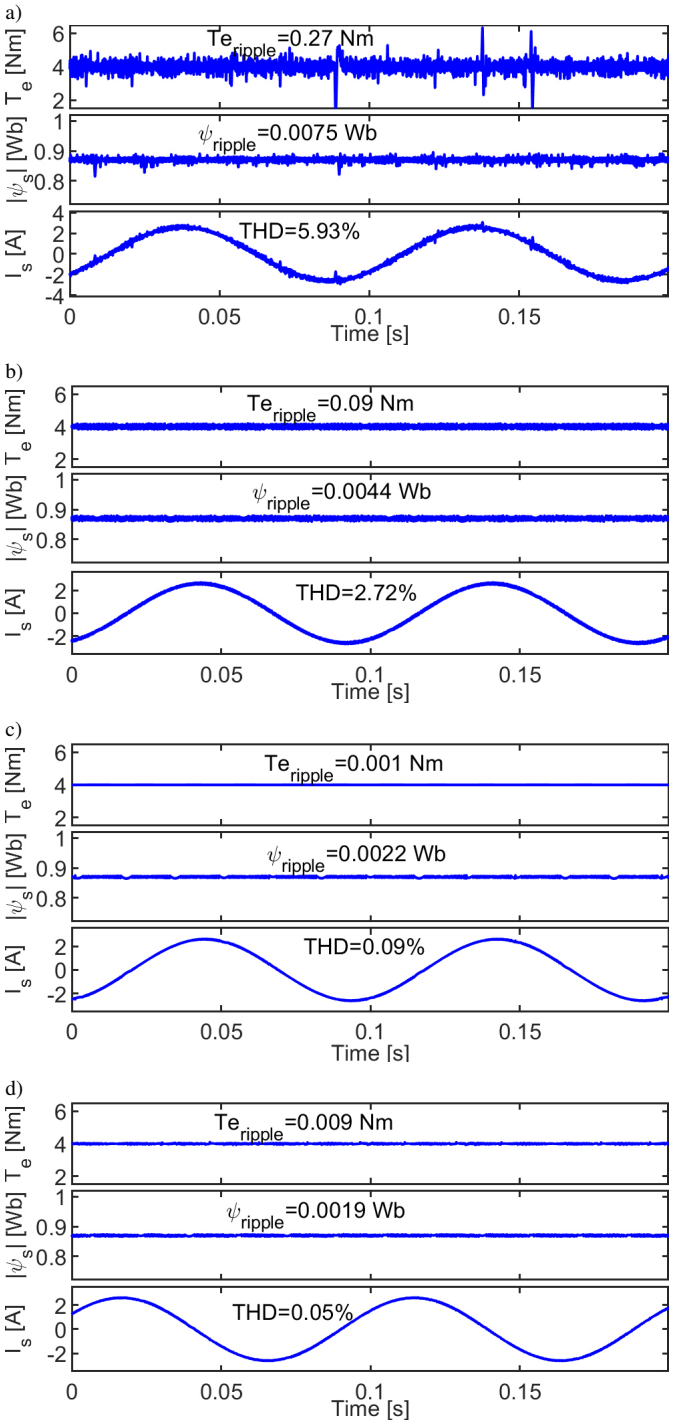

Fig. 6. Simulated steady-state response at 150 rpm with rated torque (4 Nm): a) DTC, b) MPDTC, c) Duty -MPDTC, and d) the proposed method

pared to other methods. Also, this locus accurately tracks a circular shape than that of other methods. While, a large amount of distortion exists in the stator flux locus of classical DTC, and MPDTC.

Examination results of the proposed method under different loading conditions are shown in Fig. 10. At first, the motor accelerates to the nominal speed of 1500 rpm. After the start-up stage, the nominal torque is abruptly applied to the motor at 0.15 s. The waveforms of the equivalent duty ratio, duty ratio of the first and second voltage vectors, stator current, mechanical speed, stator flux, electrical torque are presented in Fig. 10. It is revealed that the rotor speed, electrical torque and stator flux have accurately tracked the setpoint values. Meanwhile, it is observed that increasing the motor speed leads to BEMF reference; the equivalent duty ratio fluctuates between 1 and a value in the vicinity of 0.5. Also, proper portions of the equivalent duty ratio are allocated to the first and second voltage vectors.

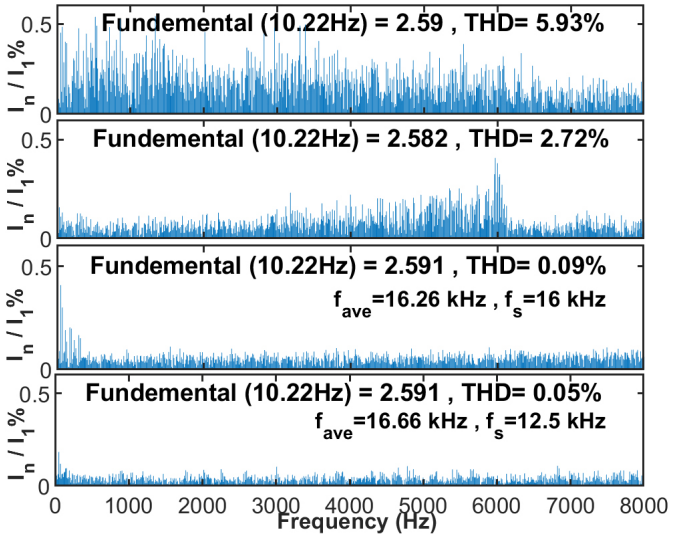

Fig. 7. Harmonics spectrum of stator current at 150 rpm with rated torque rated load from up to down for DTC, MPDTC, Duty-MPDTC, and the proposed method

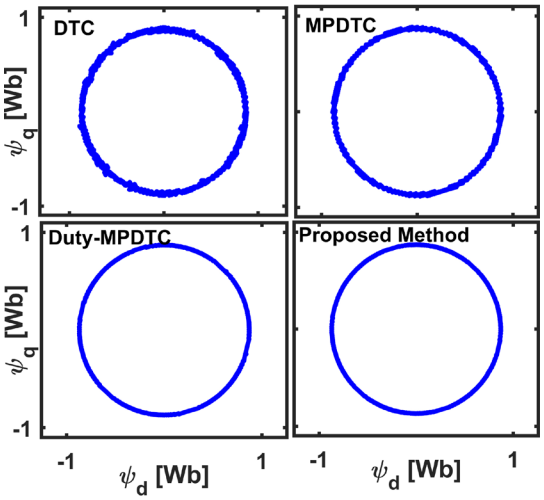

Fig. 8. Stator flux locus at 1500 rpm with rated torque (4 Nm): DTC, MPDTC, Duty-MPDTC, and the proposed method

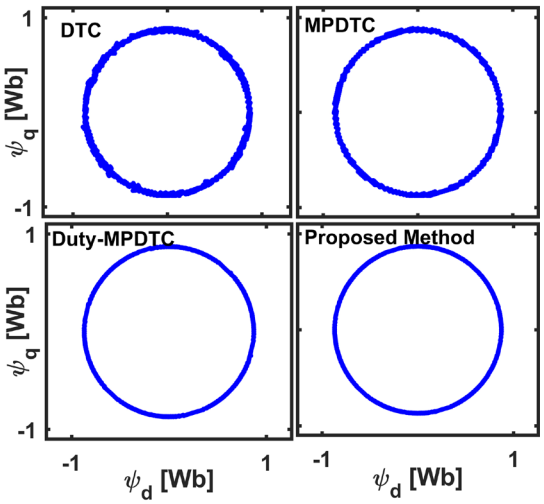

Fig. 9. Stator flux locus at 150 rpm with rated torque (4 Nm): for DTC, MPDTC, Duty-MPDTC, and the proposed method

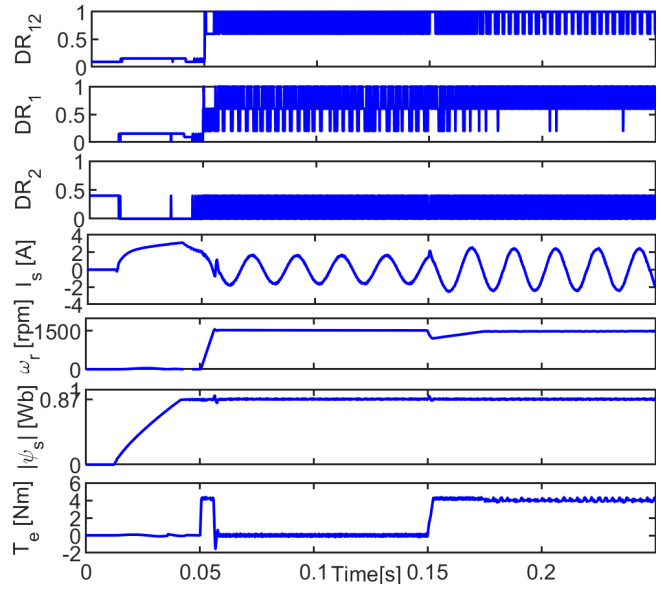

Fig. 10. Simulated waveforms of equivalent duty ratio, duty ratio the first voltage vector, duty ratio the second voltage vector, stator current, speed, stator flux, and electrical torque of the proposed method

Meanwhile, the voltage diagrams of three phases in low and high speed at nominal load have been shown in Fig. 11. Also, the voltage diagrams in the stationary $\alpha\beta$ reference frame have been shown in Fig. 12.

The responses to the abrupt exertion of mechanical torque for all understudy methods are shown in Fig. 13. While the motor

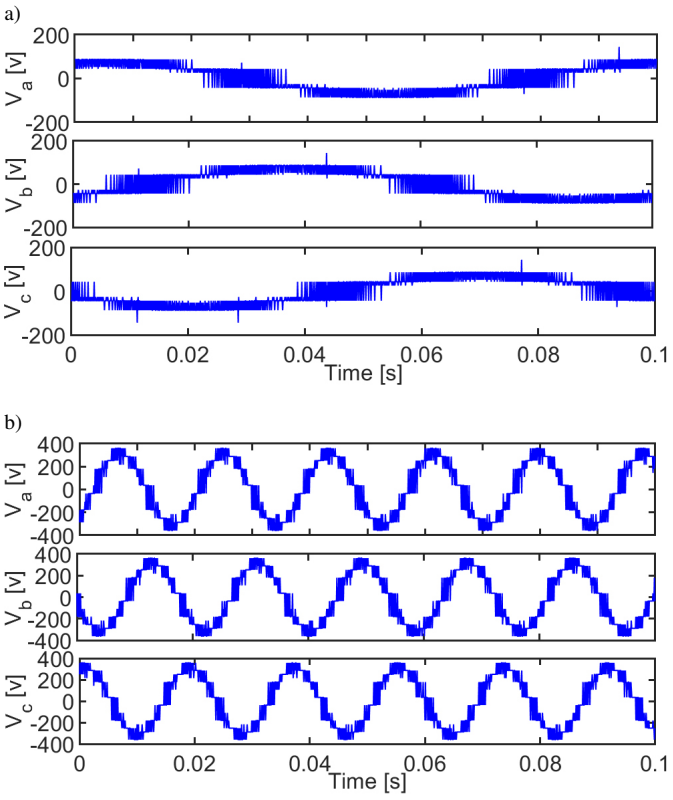

Fig. 11. Voltage diagrams of three phases in both low and high speed at nominal load

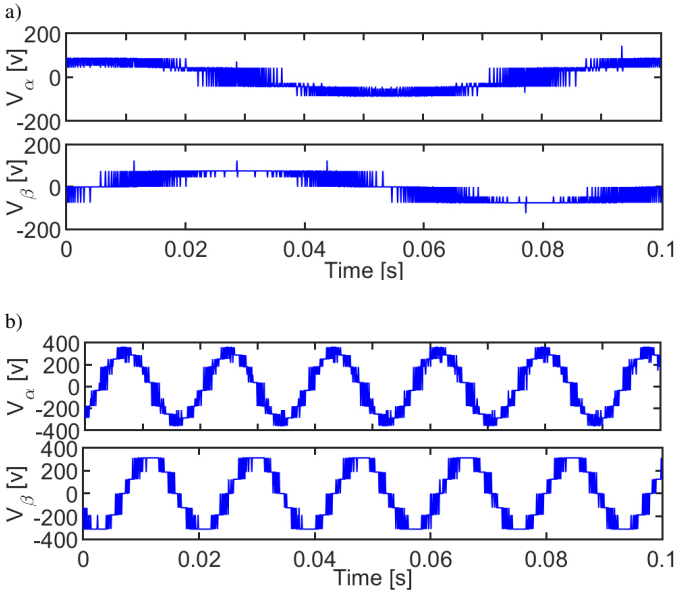

Fig. 12. Voltage diagrams in the stationary $\alpha\beta$ reference frame in both low and high speed at nominal load

rotates at 1500 rpm, a mechanical load of 4 Nm is abruptly applied to the motor. It takes a very short time until the electrical torque reaches 4 Nm for all understudy algorithms. This means that the proposed method resists the abrupt change of external load severely, and it has a very rapid dynamic performance.

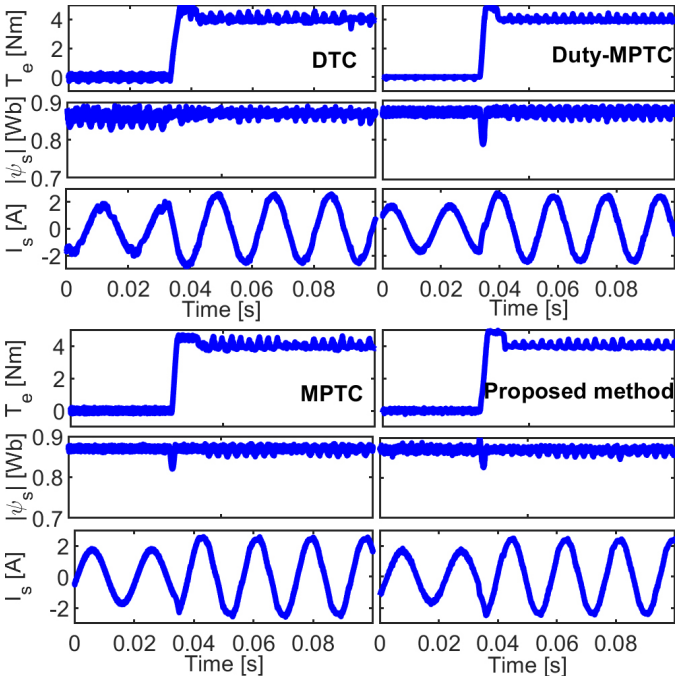

Fig. 13. Simulated dynamic operation at 1500 rpm with abrupt load change (4 Nm) for DTC, MPDTC, Duty-MPDTC, and the proposed method

The variation of current's magnitude, temperature, etc., leads to the pertinent variations in motor parameters. Hence, the sensitivity of the proposed method must be analyzed under the variations of the motor parameters. To perform the robustness analysis, the proposed method has been compared with Duty-MPDTC. The relationship of duty ratio in [34] is fully dependent on the motor parameters. The results of the robustness analysis can be seen in Fig. 14. When the motor runs at 150 rpm with 4 Nm load, stator resistance, rotor inductance, and stator inductance increase from their rated values to 150% at the instant 0.02 s. As shown in Fig. 14, torque, and speed responses of the proposed method, in comparison with Duty-MPDTC, has been not affected after the parameter variations, and the system has tracked the setpoint values after the parameter mismatches. Also, fluctuations of electrical torque are small, while, despite low torque ripple in Duty-MPDTC method due to a continuous relationship of duty ratio, electrical torque has a steady-state error and transient fluctuations with high amplitude.

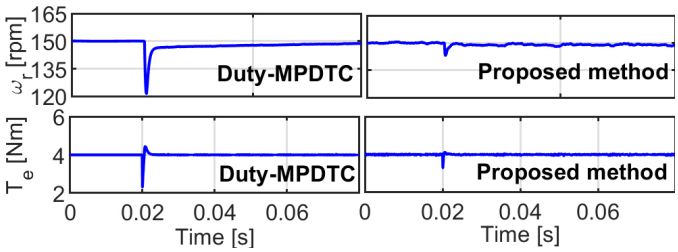

Fig. 14. Torque and speed responses at 150 rpm after 150% increment in rotor and stator inductance and stator resistance instant 0.02 s for Duty-MPDTC and the proposed method

6. IMPLEMENTATION AND EXPERIMENTAL RESULTS

Besides the simulation results, the proposed method has been experimentally evaluated on the 2L-VSI induction motor drive platform. The controller and motor parameters are the same as those listed in Table 2. The results obtained from DTC, MPDTC, Duty-MPDTC, and the proposed method have been compared. Launchpad XL TMS320F28379D, a 200 MHz and floating-point discrete signal processor board, is used to implement the understudy algorithms coded through Simulink/MATLAB. The sampling frequency for all the experiments is set to 12.5 kHz. Figure 15 shows the relevant test bench. The first experimental test has been performed under the steady-state condition when the motor runs at 1500 r/min with 4 Nm mechanical load. The waveforms of the electrical torque, stator flux, and stator current are presented in Fig. 16.

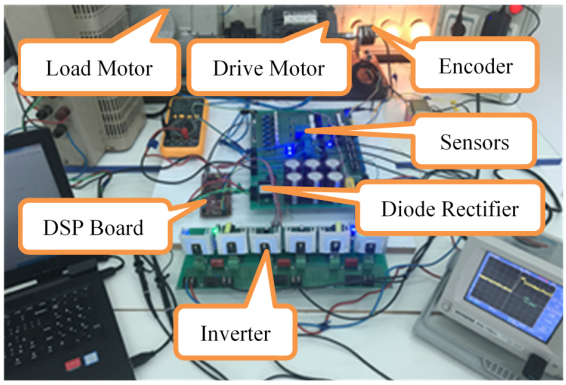

Fig. 15. Test bench of control system

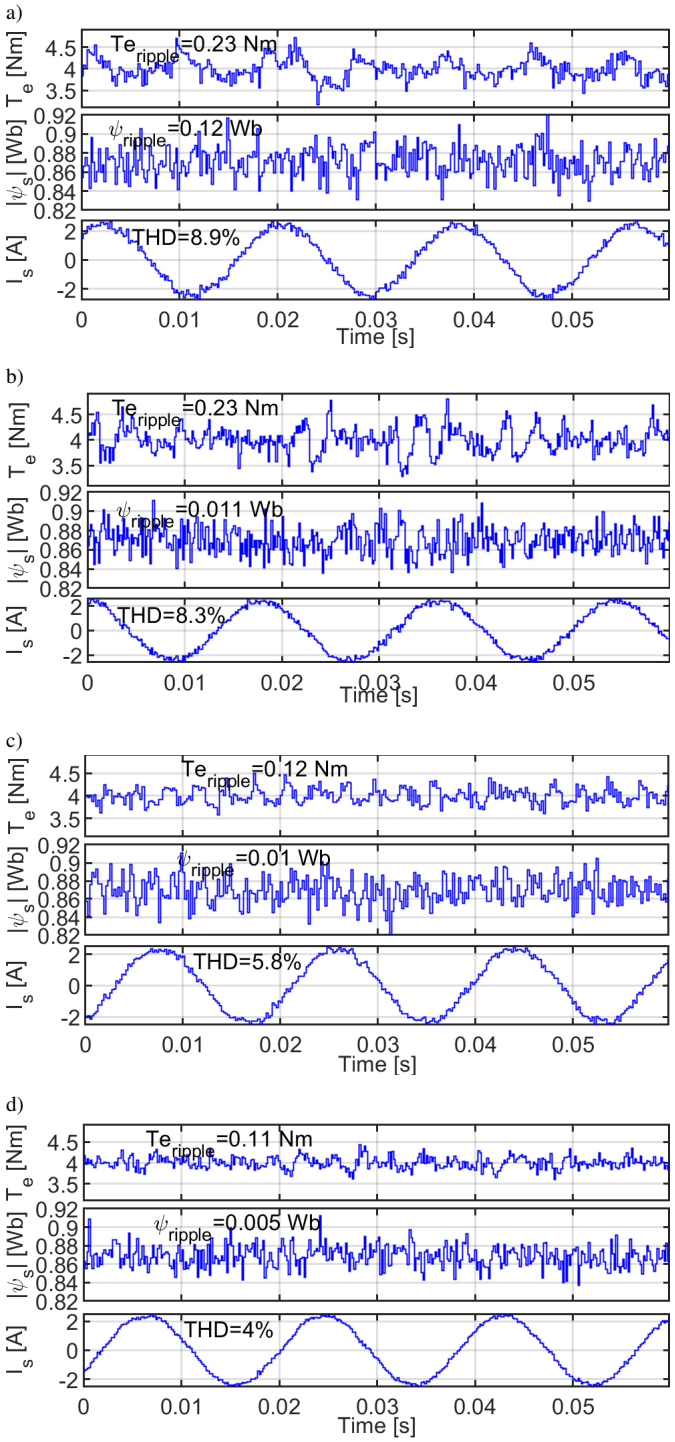

Fig. 16. Experimental steady-state response at 1500 rpm with rated torque: a) DTC, b) MPDTC, c) Duty-MPDTC, and d) the proposed method

The torque and flux ripples, as well as the current's THD are compared in Table 5. The results presented in Fig 16. indicate that the presented method has much lower flux and torque ripples and lower current THD than the other three methods, which verify the simulation study results. Figure 17 shows the dynamic state of the four methods. In this case, the motor runs at nominal speed without any mechanical load. The nominal torque (4 Nm) of the induction machine is abruptly changed. The results of full rated load disturbance indicate that the proposed method has rapidly tracked the commanding torque, like the other three methods. As depicted in Fig. 14, after exerting the mechanical load, the mechanical speed declined to around 135 rpm and returned to the setpoint values at about 8.6 ms, which is a very short time.

Table 5
Experimental results at 1500 rpm with 4 Nm load

Method	f_{ave} (kHz)	T_{e_rip} (%)	ψ_{s_rip} (%)	THD (%)
DTC	7.2	5.7	1.3	8.9
MPDTC	6.1	5.7	1.2	8.3
Duty-MPDTC	12.5	3	1	5.8
Proposed method	16.6	2.7	0.5	4.1

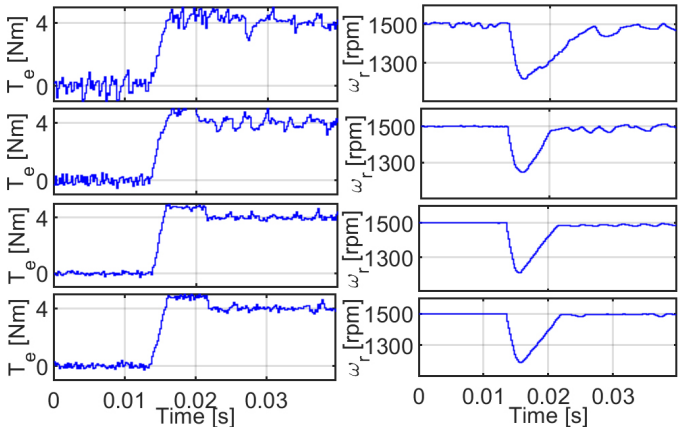

Fig. 17. After applying an abrupt load (4 Nm) from up to down for DTC, MPDTC, Duty-MPDTC, and the proposed method, respectively, experimental results of speed and torque responses were applied

7. CONCLUSION

Applying two or three vectors at each cycle control instead of one vector leads to the appearance of the best technique to reduce the torque and flux ripples in FS-MPDTC. In contrast to two-vector based MPTC, which focuses on one of the torque or flux ripples reduction, three-vector based FS-MPDTC can reduce both the torque and flux ripples at the same time due to the increase of the freedom degrees. The main conclusions drawn from the proposed strategy are given as follows:

- Unlike those methods compared with the proposed method that merely reduces the flux or torque ripples in a single speed range, the proposed method has simultaneously reduced both flux and torque ripples in all speed ranges.
- Discrete and parameter independence duty ratios are employed to enhance the robust performance of the control system.
- Duty ratios are calculated based on an intuitive and simple method.
- The calculations related to the SVM method is eliminated. In contrast, the performance of the proposed control strategy in terms of ripple reduction is similar to SVM based methods.

- The determination challenge of the classical controller in SVM based methods is eliminated by using the proposed controller.

Both the simulation and experimental results have transparently confirmed the proposed method's excellent operation compared to the conventional DTC, MPDTC and Duty-MPDTC.

REFERENCES

[1] J.P. Wach, "Maximum Torque Control of 3-phase induction motor drives," *Bull. Pol. Acad. Sci. Tech. Sci*., vol. 67, no. 2, pp. 433–445, 2018.

[2] A. Sikorski, K. Kulikowski, and M. Korzeniewski, "Modern Direct Torque and Flux Control methods of an induction machine supplied by three-level inverter," *Bull. Pol. Acad. Sci. Tech. Sci*., vol. 61, no. 4, pp. 771–778, 2013.

[3] D. Stando and M.P. Kazmierkowski, "Constant switching frequency predictive control scheme for three-level inverter-fed sensorless induction motor drive," *Bull. Pol. Acad. Sci. Tech. Sci*., vol. 68, no. 5, pp. 1057–1068, 2020.

[4] V. Talavat, S. Galvani, and M. Hajibeigy, "Direct predictive control of asynchronous machine torque using matrix converter," *Bull. Pol. Acad. Sci. Tech. Sci*., vol. 67, no. 4, pp. 773–788, 2018.

[5] I. Takahashi and T. Noguchi, "A new quick response and high efficiency control strategy of an induction motor," *IEEE Trans. Power App*., vol. IA-22, no. 5, pp. 820–827, Sept. 1986, doi: 10.1109/TIA.1986.4504799.

[6] M. Depenbrock, "Direct self-control (DSC) of a inverter fed induction machine," IEEE Trans. Power Electron., vol. 3, no. 4, pp. 420–429, Oct. 1988.

[7] Y.-S. Lai and J.-H. Chen, "A new approach to direct torque control of induction motor drives for constant inverter switching frequency and torque ripple reduction," *IEEE Trans. Energy. Convers*., vol., 16, no. 3, pp. 220–227, Sep. 2001.

[8] C. Lascu, I. Boldea, and F. Blaabjerb, "A modified direct torque control for induction motor sensorless drive," *IEEE Trans. Ind. Appl*., vol. 36, no. 1, pp. 122–130, Jan/Feb. 2000.

[9] L. Tang, L. Zhong, M. Rahman, and Y. Hu, "A novel direct torque controlled interior permanent magnet synchronous machine drive with low ripple in flux and torque and fixed switching frequency," *IEEE Trans. Ind. Appl*., vol. 19, no. 2, pp. 346–354, Mar. 2004.

[10] R. Narayan and D.B. Subudhi, "Stator inter-turn fault detection of an induction motor using neuro-fuzzy techniques," *Bull. Pol. Acad. Sci. Tech. Sci*., vol. 20, no.3, pp. 363–376, 2010.

[11] I. Bakhti, S. Chaouch, and A. Maakouf, "High performance backstepping control of induction motor with adaptive sliding mode observer," *Bull. Pol. Acad. Sci. Tech. Sci*., vol. 21, no.3, pp. 331–344, 2011.

[12] B. Kenny and R. Lorenz, "Stator- and rotor-flux-based deadbeat direct torque control of induction machines," *IEEE Trans. Ind. Appl*., vol. 39, no. 4, pp. 1093–1101, Jul/Aug. 2003.

[13] J. Rodriguez, M.P. Kazmierkowski, J. Espinoza, P. Zanchetta, H. Abu-Rub, H. Young, and C.A. Rojas, "State of the art of finite control set model predictive control in power electronics," *IEEE Trans. Ind. Inform*., vol. 9, no. 2, pp. 1003–1016, May. 2013.

[14] Y. Zhang, Y. Bai, H. Yang and B. Zhang "Low switching frequency model predictive control of three-level inverter-fed im drives with speed-sensorless and field weakening operations," *IEEE Trans. Ind. Electron*., vol. 66, no. 6, pp. 4262–4272, 2019, doi: 10.1109/TIE.2018.2868014.

[15] S.A. Davari, D.A. Khaburi, and R. Kennel, "An improved FCS-MPC algorithm for an induction motor with an imposed optimized weighting factor," *IEEE Trans. Power Electron*., vol. 27, no. 3, pp. 1540–1551, 2012.

[16] L. Yan, M. Dou, H. Zhang, and Z. Hua, "Speed sensorless dual reference frame predictive torque control for induction machines," *IEEE Trans. Power. Electron*., vol. 34, no. 12, pp. 12285–12295, 2019, doi: 10.1109/TPEL.2019.2904542.

[17] C.S. Vazquez, J. Rodriguez, M. Rivera, L.G. Franquelo, and M. Norambuena, "Model predictive control for power converters and drives: advanced and trends," *IEEE Trans. Ind. Electron*., vol. 64, no. 2, pp. 935–947, 2017.

[18] W. Xie *et al*., "Finite control set-model predictive torque control with a deadbeat solution for pmsm drives," *IEEE Trans. Ind. Electron*., vol. 62, no. 9, pp. 5402–5410, Sept. 2015, doi: 10.1109/TIE.2015.2410767.

[19] Y. Zhang, B. Yang, H. Yang, and M. Nurambuena, "Generalized sequential model predictive control of im drives with field-weakening ability," *IEEE Trans. Power Elecron*., vol. 34, no. 9, pp. 8944–8955, 2019, doi: 10.1109/TPEL.2018.2886206.

[20] M. Norambuena, J. Rodrigez, Z. Zhang, F. Wang, C. Garcia, R. Kenel, and G.-D. Andreescu, "A very simple strategy for high-quality performance of AC machines using model predictive control," *IEEE Trans. Power Electron*., vol. 34, no. 1, pp. 794–800, Jan. 2019.

[21] J. Rodriguez, R.M. Kennel, J.R. Espinoza, M. Trincado, C.A. Silva, and C.A. Rojas, "High performance control strategies for electrical drives: An experimental assessment," *IEEE Trans. Ind. Electron*., vol.29, no. 2, pp. 812– 820, Jan/Feb. 2012.

[22] T. Geyer, "Tuning guidelines for model predictive torque and flux control," *IEEE Trans. Ind. Appl*., vol. 54, no. 5, pp. 4464–4475, Oct. 2018.

[23] F. Wang, G. Lin, and Y. He, "Passivity-based model predictive control of three-level inverter-fed induction motor," *IEEE Trans. Power. Electron*., vol. 36, no. 2, pp. 1984–1993, Feb. 2021, doi: 10.1109/TPEL.2020.3008915.

[24] M. Pacas and J. Weber, "Predictive direct torque control for the PM synchronous machine," *IEEE Trans. Ind. Electron*., vol. 52, no. 5, pp. 1350–1356, Oct. 2005.

[25] F. Niu, F. Niu, K. Li, and Y. Wang, "Direct torque control for permanent-magnet synchronous machines based on duty ratio modulation," *IEEE Trans. Ind Electron*., vol. 62, no. 10, pp. 6160–6170, Oct. 2015.

[26] Y. Zhang and J. Zhu, "Direct torque control of permanent magnet synchronous motor with a reduced torque ripple and commutation frequency," *IEEE Trans. Power Electron*., vol. 26, no. 1, pp. 235–248, Jan. 2011.

[27] J.-K. Kang and S.-K. Sul, "New direct torque control of induction motor for minimum torque ripple and constant switching frequency," *IEEE Trans. Ind. Appl*., vol. 35, no. 5, pp. 1076–1082, Sep/Oct. 1999.

[28] K.K. Shyu, J.K. Lin, V.T. Pham, M.J. Yang, and T.W. Wang, "Global minimum torque ripple design for direct torque control of induction motor drives," *IEEE Trans. Ind Electron*., vol. 57, no. 9, pp. 3148–3156, Sep. 2010.

[29] Y. Ren, Z.Q. Zhu, and J. Liu, "Direct torque control of permanent-magnet synchronous machine drives with a simple duty ratio regulator," *IEEE Trans. Ind. Electron*., vol. 61, no. 10, pp. 5249–5259, Oct. 2014.

[30] Q. Liu and K. Hameyer, "Torque ripple minimization for direct torque control of pmsm with modified FSMPC," *IEEE Trans. Ind. Electron*., vol. 52, no. 6, pp. 4855–4864, Aug. 2016.

[31] Y. Zhang and H. Yang, "Torque ripple reduction of model predictive torque control of induction motor drives," in *Proc. Energy Convers. Congr. Expo*., 2013, pp. 1176–1183.

[32] Y. Zhang, H. Yang, and B. Xia, "Model predictive torque control of induction motor drives with reduced torque ripple," *IET Electr. Power Appl*., vol. 9, no. 9, pp. 595–604, 2015.

[33] Y. Zhang and H. Yang, "Model predictive torque control of induction motor drives with optimal duty cycle control," *IEEE Trans. Power Elecron*., vol. 29, no. 12, pp. 6593–6603, Dec. 2014.

[34] Y. Zhang and H. Yang, "Generalized two-vector-based Model-predictive torque control of induction motor drives," *IEEE Trans. Power Elecron*., vol. 30, no. 7, pp. 6593–6603, Jul. 2015.

[35] Y. Zhang, J. Zhu, and B. Xia, "A novel duty cycle control strategy to reduce both the torque and stator flux ripples for DTC of permanent-magnet synchronous motor drives with switching frequency reduction," *IEEE Trans. Power Electron*., vol. 31, no. 5, pp. 3738–3753, May 2016.

[36] C. Lascu and G.-D. Andreescu, "Sliding mode observer and improved integrator with dc-offset compensation for flux estimation in sensorless controlled induction motors," *IEEE Trans. Ind. Electron*., vol. 53, no. 3, pp. 785–794, Jun. 2006.

[37] P.H. Cortes, S. Kouro, B. La Rocca, R. Vargas, J. Rodrigues, J. Leon, S. Vazquez, and L. Franquelo, "Guidelines for weighting factors design in model predictive control of power converters and drives," in *Proc. IEEE ICIT*, 2009, pp. 1–7.